

True Muonium ($\mu^+\mu^-$) on the Light Front: A Toy Model

Henry Lamm* and Richard F. Lebed†

Department of Physics, Arizona State University, Tempe, AZ 85287

(Dated: November, 2013)

Applying Discretized Light Cone Quantization, we perform the first calculation of the spectrum of true muonium, the $\mu^+\mu^-$ atom, as modified by the inclusion of an $|e\bar{e}\rangle$ Fock component. The shift in the mass eigenvalue is found to be largest for triplet states. If m_e is taken to be a substantial fraction of m_μ , the integrated probability of the electronic component of the 1^3S_1 state is found to be as large as $O(10^{-2})$. Initial studies of the Lamb shift for the atom are performed. Directions for making the simulations fully realistic are discussed.

PACS numbers: 36.10.Ee, 11.10.Ef, 11.10.St, 12.20.Ds

I. INTRODUCTION

The atom consisting of a $\mu^+\mu^-$ bound state, called *true muonium* [in distinction from conventional muonium, the atom (μ^+e^-)] has not yet been identified, despite much more exotic bound states having been successfully characterized, such as $\pi\mu$ atoms [1] and even the dipositronium (e^+e^-)(e^+e^-) molecule [2]. While ($\mu^+\mu^-$) atoms have doubtless been produced many times, for example in e^+e^- colliders (where they can be easily lost in the beam line before decaying), it is only recently that immediately realizable experiments have been proposed to generate sufficient numbers of true muonium atoms to guarantee their unambiguous observation. Ideas include e^+e^- collider experiments in which the beams intersect at an angle rather than head on [thus projecting ($\mu^+\mu^-$) along the beam bisector] or conventional setups in which the produced ($\mu^+\mu^-$) recoils against a co-produced photon [3], or producing ($\mu^+\mu^-$) as a byproduct of experiments that scatter electron beams from high- Z fixed targets in search of hidden-sector *heavy photons* [4].

True muonium consists of a spectrum of metastable states (lifetimes in the ps to ns range [3]), for which the 2.2 μ s muon weak decay lifetime is effectively infinite. The transitions are therefore overwhelmingly electromagnetic, meaning that ($\mu^+\mu^-$) can be treated, like positronium (e^+e^-), as a Bohr atom [in the ($\mu^+\mu^-$) case, with a ground-state radius of only 512 fm], and its transitions can be computed using QED. Unlike positronium, its decay products include not only monochromatic photons, but also e^+e^- pairs of well-characterized energies. Studies of ($\mu^+\mu^-$) are further motivated by discrepancies in precision muon-related effects, such as $(g-2)_\mu$ and the proton charge radius [5, 6].

As far as an isolated ($\mu^+\mu^-$) bound state is concerned, conventional QED and quantum-mechanical wave functions are generally sufficient to compute its most important features, just as is true for (e^+e^-). However, these techniques provide not as much guidance for understanding the detailed structure-dependent dynamics

of the atoms. Indeed, remarkable experiments can in principle be performed on these “atoms in flight”, including measurements of the Lamb shift [7]. Bound states in quantum field theory (QFT) are notoriously complicated objects, due not only to the fact that the vacuum consists of an arbitrarily large number of virtual particles, but also because the constituents can be relativistic, and the required boosts to relate the components of the wave function depend in a detailed way upon the interaction.

In fact, a well-known method of studying bound states avoids these problems. By performing quantization not, as usual, with respect to conventional time t (called *instant form*) but rather with respect to the light-front time $x^+ \equiv t + z$ (called *front form*) [8], one develops a Hamiltonian formalism that is nonetheless fully covariant and ideally suited to characterizing bound states comprised of well-defined constituents [9]. The analogue to a Schrödinger equation for the state then becomes an infinite but denumerable set of coupled integral equations. In order to obtain numerical results, one may then truncate the equations by limiting the set of component Fock states included in the calculation and discretizing momenta with suitable periodic boundary conditions, effectively turning infinite-dimensional matrices into finite ones and creating a problem solvable on a computer, which is termed Discretized Light-Cone Quantization (DLCQ) [10].

Our purpose in this article is to report on the first simulation of the true muonium atom using DLCQ and other light-front techniques. We borrow heavily on older works that use this approach to simulate positronium. The first such attempt [11] was impeded by slow numerical convergence, which was successfully addressed by a better treatment [12] of the singularity induced by the Coulomb interaction. Further work [13] superseded the effective interaction approach of [12] to perform a direct diagonalization of the Hamiltonian matrix. The work of Trittmann and Pauli [14] unified these improvements, and additionally included in the Fock space the explicit single-photon annihilation channel $|\gamma\rangle$. They also demonstrated the numerical restoration of rotational invariance, a needed improvement since light-front coordinates treat the longitudinal and transverse directions very differently. Our work is a direct application of the methods introduced

* hlamniv@asu.edu

† Richard.Lebed@asu.edu

in Ref. [14] to true muonium; our principal innovation, apart from the trivial substitution of the valence electrons with muons, is the inclusion of $|e\bar{e}\rangle$ Fock states, which can mix with the $|\mu\bar{\mu}\rangle$ component via the explicit $|\gamma\rangle$ component.

The positronium simulations of Ref. [14] adopted the unphysically large value $\alpha = 0.3$ in order to show the robustness of the method at large values of coupling, where high-order QED calculations begin to become unreliable. An additional purpose for this choice was to provide numerical evidence that strong-coupling DLCQ would be applicable to the much more intricate QCD bound-state problem. In our calculations presented here, we maintain this large value of α in order to study the effects of a large $|e\bar{e}\rangle$ component of true muonium; of course, α is an adjustable parameter of the program and can be altered for more physical simulations in our future work. Moreover, the code designed by Ref. [14] contains only one fermion mass parameter, m_e in their case and m_μ in ours. In the present work, m_e is an independent parameter; again, to study the effects of a large $|e\bar{e}\rangle$ component, we allow m_e to be any finite fraction of m_μ . Ultimately, for physical applications one sets $m_e/m_\mu \simeq 4.8 \cdot 10^{-3}$, but we exhibit results with $m_e/m_\mu = O(1)$ for the practical reason that properly characterizing a system in QFT with two widely separated scales requires proper renormalization evolution between the scales (In front form, the original diagrammatic renormalization techniques are described in Ref. [15]). Since the evolution typically depends upon the log of the ratio of scales, choosing m_e not excessively small compared to m_μ minimizes this effect; we plan to address this important issue thoroughly in a subsequent paper [16].

Even with a large $|e\bar{e}\rangle$ component, our simulations reproduce the Bohr spectrum of true muonium to a high degree of precision. Nevertheless, the significance of the $|e\bar{e}\rangle$ component is clearly seen in the true muonium eigenvalues, and especially in the wave functions. We also see modifications to the $(\mu^+\mu^-)$ Lamb shift in agreement with their expected dependence upon the atom's principal quantum number n . While the proper numerical and formal treatment of the $|e\bar{e}\rangle$ sector will require future improvements (the effects of neglecting which are exhibited below), we find these initial results to be very encouraging.

This paper is organized as follows. In Sec. II, we present essential conceptual and formal details of light-front bound-state techniques relevant to this work, and describe the associated numerical details in Sec. III. We define our model in Sec. IV and discuss the effects of the $|e\bar{e}\rangle$ component in Sec. V. Section VI provides a discussion of the effect of momentum-space cutoffs. We present our results in Sec. VII, with conclusions in Sec. VIII and details of the calculation of the relevant matrix elements in the Appendix.

II. LIGHT-FRONT BOUND STATES

The action-functional approach has become the predominant method for performing QFT calculations. It is based upon a Lorentz-invariant Lagrangian density, and the symmetries of the theory (including gauge invariance) can be incorporated very efficiently. On the other hand, the Hamiltonian formalism provides a more natural language for describing bound-state systems, just as it does in non-relativistic quantum mechanics. However, Hamiltonians are complicated objects in relativistic QFT, especially in the instant form: The nonanalytic nature of the operator $\sqrt{\mathbf{P}^2 + M^2}$ causes difficulties; the constituent particles have distinct rest frames, and the boost operations necessary to express them as part of a single wave function depend intrinsically upon the interactions between them; and most significantly, the vacuum structure is exceedingly complicated due to the creation and annihilation of virtual states with arbitrarily large numbers of quanta.

The front form addresses each of these difficulties. First, the Hamiltonian operator $P^- \equiv P^0 - P^3$ conjugate to the time coordinate x^+ is related linearly to the energy-squared operator,

$$H_{LC} = P^- P^+ - \mathbf{P}_\perp^2, \quad (1)$$

where $P^+ \equiv P^0 + P^3$ is the longitudinal momentum component conjugate to the light-front longitudinal direction $x^- \equiv t - z$, and the transverse momentum is $\mathbf{P}_\perp \equiv P^1 \mathbf{x} + P^2 \mathbf{y}$. For an eigenvalue M^2 of the operator H_{LC} corresponding to a state $|\Psi\rangle$, the light-front Hamiltonian eigenvalue equation is no longer nonanalytic:

$$P^- |\Psi\rangle = \frac{M^2 + \mathbf{P}_\perp^2}{P^+} |\Psi\rangle. \quad (2)$$

Second, out of the 10 Poincaré generators P^μ and $M^{\mu\nu}$, the front form is special in having 7 that leave the time slice $x^+ = \text{const}$ invariant [8], and therefore can be expressed without reference to the specific interaction in the Hamiltonian. These so-called *kinematic* operators are the spatial momentum components \mathbf{P}_\perp , P^+ , the longitudinal angular momentum ($M^{12} = J_z$) and boost ($M^{+-} = K_z$) generators, and the mixed transverse-longitudinal boosts $M^{+\perp}$. In contrast, the instant form has only 6 kinematic operators: the spatial momentum P^i and angular momentum M^{ij} components; in particular, the boost generators M^{0i} are all *dynamic*, in that they depend upon the interaction. Although the front form addresses the boost issue by providing kinematic boost generators, the price is the loss of manifest rotational invariance (the absence of simple \mathbf{J}_\perp generators), which is apparent from the fact that front form treats x^3 differently from $x^{1,2}$. The P^μ and total spin operators S^2 and S_z still commute in front form, meaning that a particular state $|\Psi\rangle$ can be completely specified as

$$|\Psi; M, P^+, \mathbf{P}_\perp, S^2, S_z; h\rangle, \quad (3)$$

where h indicates any discrete or non-spacetime quantum numbers, such as parity or lepton number.

Third, and most significantly, the numerical values of longitudinal momenta P^+ for all physical particles are nonnegative, since $P^0 = E > P^3$. One cannot create virtual particles traveling “backwards” with respect to the light-front longitudinal direction, so empty space cannot produce collections of virtual particles in front form, in stark contrast to the situation in instant form. The ground state of the free theory is also the ground state of the full interacting theory, and the Fock state expansion built upon the free vacuum provides a rigorous “parton” component description of the full interacting state.

To be specific, the state $|\Psi\rangle$ may be expressed in terms of its Fock components $|\mu_n\rangle$, where n in general is denumerably infinite. Each particular component $|\mu_n\rangle$ contains a fixed number N_n of constituent quanta, the i^{th} of which has rest mass m_i and momentum k_i^μ (out of the total momentum P^μ). The kinematics may alternatively be described in terms of longitudinal boost-invariant quantities $x_i \equiv k_i^+/P^+$ ($0 \leq x_i \leq 1$) and $\mathbf{k}_{\perp i}$, and helicities λ_i , so that

$$\sum_{i=1}^{N_n} x_i = 1, \quad \sum_{i=1}^{N_n} \mathbf{k}_{\perp i} = \mathbf{P}_\perp, \quad (4)$$

and, working in the *intrinsic frame*, in which $\mathbf{P}_\perp = 0$,

$$k_i^\mu = \left(x_i P^+, \mathbf{k}_{\perp i}, \frac{m_i^2 + \mathbf{k}_{\perp i}^2}{x_i P^+} \right). \quad (5)$$

Using the completeness of the states $|\mu_n\rangle$, the decomposition then reads

$$\begin{aligned} |\Psi\rangle &\equiv \sum_n \int [d\mu_n] |\mu_n\rangle \langle \mu_n | \Psi; M, P^+, \mathbf{P}_\perp, S^2, S_z; h \rangle \\ &\equiv \sum_n \int [d\mu_n] |\mu_n\rangle \Psi_{n|h}(\mu), \end{aligned} \quad (6)$$

where the measure notation indicates an integration over values of all constituent x_i, \mathbf{k}_\perp , subject to the constraints of Eq. (4). The functions $\Psi_{n|h}(\mu)$, where now h and μ are shorthand for all the intrinsic and kinematic quantum numbers, respectively, of the Fock state n , are called the *component wave functions* of the state and are the central objects of interest in bound-state light-front calculations. The Hamiltonian expression Eq. (2) then becomes

$$\begin{aligned} &\sum_{n'} \int [d\mu_{n'}] \langle \mu_n : x_i, \mathbf{k}_{\perp i}, \lambda_i | P^- | \mu_{n'} : x'_i, \mathbf{k}'_{\perp i}, \lambda'_i \rangle \\ &\quad \times \Psi_{n'|h}(x'_i, \mathbf{k}'_{\perp i}, \lambda'_i) \\ &= \frac{M^2 + \mathbf{P}_\perp^2}{P^+} \Psi_{n|h}(x_i, \mathbf{k}_{\perp i}, \lambda_i), \end{aligned} \quad (7)$$

which is an exact infinite-dimensional integral equation for the component wave functions $\Psi_{n|h}(\mu)$. Although this expression has been derived from a full QFT with no approximations, one may identify it as the light-front

version of the Schrödinger equation. Specifically, the kinetic energy operator for the i^{th} component in the frame $\mathbf{P}_\perp = 0$ reads

$$T_i = \frac{m_i^2 + \mathbf{k}_{\perp i}^2}{x_i}, \quad (8)$$

and the bound-state equation for two equal-mass valence particles interacting via the effective potential V_{eff} is described by the integral equation

$$\begin{aligned} &\left(M^2 - \frac{m^2 + \mathbf{k}_\perp^2}{x(1-x)} \right) \psi(x, \mathbf{k}_\perp; \lambda_1, \lambda_2) \\ &= \sum_{\lambda'_1, \lambda'_2} \int_D dx' d^2 \mathbf{k}'_\perp \langle x, \mathbf{k}_\perp; \lambda_1, \lambda_2 | V_{\text{eff}} | x', \mathbf{k}'_\perp; \lambda'_1, \lambda'_2 \rangle \\ &\quad \times \psi(x', \mathbf{k}'_\perp; \lambda'_1, \lambda'_2). \end{aligned} \quad (9)$$

The appearance of reciprocal powers of momenta in Eq. (2), which is the ultimate origin of the singularities at $x = 0$ or 1 in Eq. (9), requires a careful regularization of numerical integrals. The domain D in Eq. (9) is defined by introducing a cutoff Λ on the parton transverse momentum \mathbf{k}_\perp ; in the equal-mass case, we choose [17]

$$\frac{m^2 + \mathbf{k}_\perp^2}{x(1-x)} \leq \Lambda^2 + 4m^2. \quad (10)$$

Instituting a momentum-space cutoff has the added effect of minimizing the influence of multiparticle Fock states. In principle, each sector of the theory (in our case, notably $\mu\bar{\mu}$ and $e\bar{e}$) can have an independent cutoff, but such choices must be motivated by the physical scales of the problem, and in any case the final results must eventually be insensitive to such particular choices. We discuss these issues in greater detail in Sec. VI.

For a gauge theory like QED, the light-cone gauge $A^+ = 0$ is the most natural choice because it eliminates the spatial non-transverse modes. Using the equations of motion, one may then eliminate the A^- component in favor of the other fields in the theory; this inversion is subtle due to the existence of “zero modes” of A^+ , but such modes are not expected to affect the spectrum of bound states in a crucial way [14]. The result is a fairly complicated but closed-form exact Hamiltonian that may be used to develop front-form Feynman rules [9, 17].

The Hamiltonian can be described by the sum of Feynman rules for a kinetic operator T and various types of interactions: *seagulls* S [including their normal-ordered *contractions*], which do not change particle number, *vertices* V , which change particle number by one, and *forks* F , which change particle number by two:

$$H_{\text{LC}} = T + S + V + F. \quad (11)$$

The exact form of each operator has been worked out and can be found in many places, *e.g.*, in Ref. [9]. The connection of the lowest Fock states by these interactions for true muonium is summarized in Table I.

Sector	n	0	1	2	3	4	5	6	7	8
$ \gamma\rangle$	0	•	V	V	•	F	F	•	•	•
$ e\bar{e}\rangle$	1	V	•	S	S	V	•	F	•	F
$ \mu\bar{\mu}\rangle$	2	V	S	•	S	•	V	•	F	F
$ \gamma\gamma\rangle$	3	•	S	S	•	V	V	•	•	•
$ e\bar{e}\gamma\rangle$	4	F	V	•	V	•	S	V	•	V
$ \mu\bar{\mu}\gamma\rangle$	5	F	•	V	V	S	•	•	V	V
$ e\bar{e}e\bar{e}\rangle$	6	•	F	•	•	V	•	•	•	S
$ \mu\bar{\mu}\mu\bar{\mu}\rangle$	7	•	•	F	•	•	V	•	•	S
$ \mu\bar{\mu}e\bar{e}\rangle$	8	•	F	F	•	V	V	S	S	•

TABLE I. The Hamiltonian matrix for two-flavor QED, where n labels Fock states. The vertex, seagull and fork interactions are denoted by V, S, F respectively. Diagonal matrix elements are indicated by •, and vanishing matrix elements by a •.

In order to reduce Eq. (7) to a finite-dimensional equation that can be solved numerically [in particular, the form Eq. (9)], the space of included Fock states $\{|F\rangle\}$ must be truncated. The straightforward approach of using the fundamental interactions of $\{|F\rangle\}$ alone and ignoring all others $\{|\bar{F}\rangle\}$ is called the *Tamm-Dancoff method* [18, 19]. Unfortunately, this approach can easily sacrifice Lorentz covariance or gauge invariance; including the effect of higher Fock states $\{|\bar{F}\rangle\}$ to restore the necessary structures is the aim of the *method of iterated resolvents* [20], which treats $\{|\bar{F}\rangle\}$ as giving rise to effective interactions among the states $\{|F\rangle\}$ [which, in Eq. (9), contribute to V_{eff}]. Since only the complete theory (QED in our case) with arbitrarily complicated Fock states that are precisely related by the exact Lagrangian can uniquely specify the correct effective interaction, the iterated resolvents simply act to provide one minimal completion of the interaction, written exclusively in terms of $\{|F\rangle\}$.

III. NUMERICAL SIMULATION ON THE LIGHT FRONT

To solve Eq. (9), one can discretize the momentum-space Fourier modes and solve the resulting eigenvalue problem on a finite grid (the DLCQ method). Discretization in (x, \mathbf{k}_\perp) space results in an asymmetric matrix, which significantly increases the computational effort, so one may instead use a set of variables (μ, θ, ϕ) defined by

$$x = \frac{1}{2} \left(1 + \frac{\mu \cos \theta}{\sqrt{m_i^2 + \mu^2}} \right), \quad (12)$$

$$\mathbf{k}_\perp = \mu(\sin \theta \cos \phi, \sin \theta \sin \phi, 0). \quad (13)$$

Using these variables, one may exchange ϕ for the discrete quantum number J_z [14] and compute using only

μ, θ . The new variable μ can be considered an off-shell mass, due to the relation

$$\frac{m_i^2 + \mathbf{k}_\perp^2}{x(1-x)} = 4(\mu^2 + m_i^2). \quad (14)$$

Since these coordinates depend upon the fermion mass m_i , different sets of μ, θ values result from the same sets of x and \mathbf{k}_\perp values in the two-flavor system.

To discretize, we utilize the Gauss-Legendre method for both μ and θ . The μ range is $[0, \frac{\Lambda_i}{2}]$, where Λ_i is the momentum cutoff for flavor i (see Sec. VI), and $\cos \theta \in [-1, 1]$. To allow for values $\Lambda_i \rightarrow \infty$, we remap the interval to one $\in [0, 1]$ via a weighting

$$f(\mu) = \frac{1}{1 + \mu}, \quad (15)$$

where μ here is expressed in units of the Bohr momentum $\alpha m_i/2$. With reference to Eq. (12), if one fixes the cutoff Λ_i and increases the number of sampling points N_μ , this mapping f then places more grid points at low μ to better sample the wave function around $x = \frac{1}{2}$, and high μ to better sample around $x = 0, 1$. From this scheme, one sees that four numbers essentially determine the quality of numerical calculation: the number of sampling points N_μ and N_θ , and the momentum cutoffs Λ_μ and Λ_e . While the number of sampling points N_μ, N_θ are independent, for the entirety of this work they are set equal, $N_\mu = N_\theta = N$.

The $1/q^2$ singularity introduced by the Coulomb interaction, where \mathbf{q} is the momentum transfer, is handled by the same *counterterm method* as described in Ref. [14] and first implemented in Ref. [12]: The discrete matrix elements near the singularity are replaced by a continuous (and convergent) integral. The only necessary modification in the two-flavor case is to use separate counterterms in each flavor sector.

IV. TRUE MUONIUM MODEL

Our model simply uses QED with two fermion flavors, the electron e and the muon μ , but in which the “electron” is dramatically heavier than its physical value of $m_e/m_\mu \simeq 4.8 \cdot 10^{-3}$, in order to explore the effect of the extra flavor sector beyond a simple “scaled-up” version of positronium. Nevertheless, the condition $m_e < m_\mu$ is always imposed, and as mentioned above, we set $\alpha = 0.3$ to enhance the effects of the extra sector. In this basis, one can express the state of all possible charge-zero, lepton family-number zero wave functions defined by:

$$|\Psi\rangle = \psi_{\mu\bar{\mu}}|\mu\bar{\mu}\rangle + \psi_{e\bar{e}}|e\bar{e}\rangle + \psi_\gamma|\gamma\rangle + \psi_{\mu\bar{\mu}\gamma}|\mu\bar{\mu}\gamma\rangle + \psi_{e\bar{e}\gamma}|e\bar{e}\gamma\rangle + \dots \quad (16)$$

The full physical problem would require not only decreasing m_e and α , but also including hadronic polarization corrections to the photon propagators.

In this initial model of true muonium, we extend the Fock space considered in Refs. [14, 21–23] to include a second flavor of fermions: $|\mu\bar{\mu}\rangle$, $|\mu\bar{\mu}\gamma\rangle$, $|e\bar{e}\rangle$, $|e\bar{e}\gamma\rangle$, and $|\gamma\gamma\rangle$. Through a proper choice of effective interactions [24], one can truncate the Fock space at these states and neglect other Fock states such as $|\gamma\gamma\rangle$ or $|\mu\bar{\mu}e\bar{e}\rangle$ in a self-consistent way. The $|e\bar{e}\rangle$ states are of particular interest because their continuum states constitute the dominant decay mode of the 3S_1 ($C = -1$) states of true muonium. Furthermore, its inclusion in the numerical simulation (along with $|e\bar{e}\gamma\rangle$) is straightforward because it requires no conceptual innovation beyond that used to study the $|\mu\bar{\mu}\rangle$ and $|\mu\bar{\mu}\gamma\rangle$ states; the only complication is that the matrices to be diagonalized become much larger, increasing computation time.

Solving for the eigenstates of H_{LC} with this limited Fock space nonetheless gives the bound states of positronium ($e\bar{e}$) and true muonium ($\mu\bar{\mu}$), as well as the continuum states of γ , $e\bar{e}$, and $\mu\bar{\mu}$, exactly (up to the effects due to the neglected higher-order Fock states). The output of this calculation is the wave functions of various helicity states for $|\mu\bar{\mu}\rangle$ and $|e\bar{e}\rangle$ components ψ in the form of Eq. (9), *i.e.*, with the γ components folded into V_{eff} by means of the method of iterated resolvents.

V. EFFECT OF THE $|e\bar{e}\rangle$ SECTOR

Proper inclusion of the front-form Fock states $|e\bar{e}\rangle$ and $|e\bar{e}\gamma\rangle$ should replicate the physics in instant form due to the inclusion of instant-form diagrams with an e^+e^- pair and a γ , such as vacuum polarization due to electrons in the single-photon annihilation channel (called VP-e-A in Ref. [25]). The importance of including both $|e\bar{e}\rangle$ and $|e\bar{e}\gamma\rangle$ states in our simulations is twofold.

First, the dominant decay channel for true muonium in 3S_1 states is e^+e^- production, while the dominant decay channel for 1S_0 ($C = +1$) states is $\gamma\gamma$. Note that the well-known leading-order result for the 3S_1 - 1S_0 hyperfine splitting, $\Delta E = \frac{7}{12}m_\mu\alpha^4$ for true muonium, has been derived analytically in front form [26, 27], so that other physical effects sensitive to small $\mu^+\mu^-$ separation such as $\mu^+\mu^- \rightarrow \gamma \rightarrow e^+e^-$ should also be considered.

While including the $|e\bar{e}\rangle$ state into our calculations requires essentially nothing but duplicating the $|\mu\bar{\mu}\rangle$ states as $|e\bar{e}\rangle$ and computing one new set of matrix elements (see Appendix), properly including a $|\gamma\gamma\rangle$ state would require computing many new matrix elements, developing new counterterms to regularize singular integrals, and properly renormalizing the photon mass terms that arise on the light front. We plan to address these issues in future work.

Second, Jentschura *et al.* [25] showed in instant form that VP-e-A is the second-largest correction to the hyperfine splitting in true muonium. The only correction that is larger in instant form arises from vertex corrections, which are partly incorporated in front form through the inclusion of $|\mu\bar{\mu}\gamma\rangle$ states, but can be fully treated only

through proper renormalization. Furthermore, Ref. [25] finds the energy shifts arising from the $|\gamma\gamma\rangle$ states to be several times smaller than those from either VP-e-A or vertex corrections. The calculations of Ref. [25] rely upon the asymptotic behavior of the vacuum polarization, which for true muonium is the limit of $m_e/m_\mu \ll 1$. In our case of $m_e/m_\mu = O(1)$, one might expect significant corrections to the asymptotic behavior. To find the effect of these corrections, one can compute the exact correction due to VP-e-A without the asymptotic approximation. As first shown in [28], the leading-order radiative correction to the QED particle-antiparticle bound-state energy spectrum due to a virtual fermion loop coupling to the electromagnetic field with amplitude φ_0 (which, in the nonrelativistic limit, is just the wave function) is

$$\begin{aligned} \Delta E_{\text{VP}} &= \frac{\pi\alpha}{m_i^2} \left(1 - \frac{4\alpha}{\pi}\right) \bar{\Pi}^R(4m_i^2) |\varphi_0|^2 \langle \mathbf{S}^2 \rangle + O(\alpha^6) \\ &= \frac{\alpha^4 m_i}{4n^3} \left(1 - \frac{4\alpha}{\pi}\right) \bar{\Pi}^R(4m_i^2) + O(\alpha^6), \end{aligned} \quad (17)$$

where m_i is the mass of the bound fermion, $\bar{\Pi}^R(q^2)$ is the renormalized polarization function, and \mathbf{S}^2 is the total spin Casimir operator. In the second line we have specialized to the $n {}^3S_1$ state, for which $|\varphi_0|^2 = m_i^3 \alpha^3 / 8\pi n^3$ is the nonrelativistic squared wave function at the origin, and $\langle \mathbf{S}^2 \rangle = 2$. The exact form of the one-loop vacuum polarization function is

$$\bar{\Pi}^R(q^2) = \frac{\alpha}{3\pi} \left[-\frac{5}{3} - \frac{4m_f^2}{q^2} + \left(1 + \frac{2m_f^2}{q^2}\right) f(q^2) \right], \quad (18)$$

where m_f is the mass of the loop fermions, and the form of $f(q^2)$ depends upon whether q^2 is spacelike or timelike and its size compared to $4m_f^2$. In the region $4m_f^2 < q^2$, *e.g.*, for true muonium with electron-loop corrections, one finds

$$f(q^2) = \sqrt{1 - \frac{4m_f^2}{q^2}} \ln \left(\frac{1 + \sqrt{1 - \frac{4m_f^2}{q^2}}}{1 - \sqrt{1 - \frac{4m_f^2}{q^2}}} \right) - i\pi \sqrt{1 - \frac{4m_f^2}{q^2}}, \quad (19)$$

where the imaginary term signals the possibility for decay. Inserting Eqs. (18)–(19) into Eq. (17), taking the $m_e \rightarrow 0$ limit, and dropping the $O(\alpha^6)$ terms, we reproduce Eq. (26) of [25], which we express slightly differently as

$$\begin{aligned} \Delta E_{\text{VP}}(n^3 S_1) &= \frac{m_\mu \alpha^5}{4\pi n^3} \left[\frac{1}{3} \ln \left(\frac{4m_\mu^2}{m_e^2} \right) - \frac{5}{9} - \frac{i\pi}{3} \right. \\ &\quad \left. + O \left(\frac{m_e^2}{4m_\mu^2}, \alpha \right) \right]. \end{aligned} \quad (20)$$

In typical cases considered here ($m_e/m_\mu \sim 0.1$ – 0.8), this expansion predicts relative corrections to the asymptotic form of order 10%, so the complete formulas [Eqs. (17)–(19)] are retained for our numerical results.

In order to compare our results to those of instant-form perturbation theory calculations, we compare shifts in M^2 :

$$\begin{aligned} \Delta M^2 &\equiv M_{\mu\mu}^2 - M_0^2 \\ &= (2m_\mu + B + \Delta E)^2 - (2m_\mu + B)^2, \end{aligned} \quad (21)$$

where $M_{\mu\mu}^2$ is the squared mass of our model true muonium including the $|e\bar{e}\rangle$ component, while M_0^2 is the squared mass neglecting the electron Fock states, ΔE is the total binding energy due to the presence of the $|e\bar{e}\rangle$ states, and B is the remaining binding energy terms of the atom. In Sec. VII we examine how well taking $\Delta E = \Delta E_{\text{VP}-e-A}$, where the latter refers to the original instant-form expression of Eq. (17), matches the light-front results.

VI. CUTOFF AND RENORMALIZATION ISSUES

In front form, the most common renormalization scheme for two-body systems is the covariant cutoff approach of Lepage and Brodsky [17]:

$$\frac{m^2 + \mathbf{k}_\perp^2}{x(1-x)} \leq \Lambda^2 + 4m^2. \quad (22)$$

Unfortunately, in any but the simplest models, this formulation does not properly renormalize the Hamiltonian as new sectors are added. More recent attempts to utilize other renormalization schemes include Pauli-Villars [29, 30] and Hamiltonian flow [31, 32] techniques, and methods with sector-dependent counterterms [33, 34].

For the purposes of this work, we take the simplest possible renormalization scheme by defining two covariant cutoffs via Eq. (22): Λ_μ for the muon sector and Λ_e for the electron sector. In future work we will address the question of renormalization in true muonium in much greater detail.

To investigate the effect of this choice of cutoffs, we first fix $\Lambda_e = \frac{m_e}{m_\mu} \Lambda_\mu$ [to achieve parallel forms of Eq. (22) for the two sectors] and vary $1 \leq \Lambda_\mu \leq 65$ (in units of muon Bohr momentum $\alpha m_\mu/2$). Results for the $n = 1, 2$ eigenstates with $m_e = \frac{1}{2}m_\mu$ can be seen in Figs. 1 and 2, respectively, which can be compared to Figs. 2.8 and 2.9 of Ref. [14], where the same study was performed for positronium. Since rotational invariance is obscured in the front form, states studied in the numerical simulations are labeled by adding the J_z label, as in $n^{2S+1}L^{J_z}$.

In the positronium case, a 2^1S_0 - 2^3P_0 level crossing was seen in the range $1.5 \leq \Lambda_\mu \leq 7$. In contrast, in our true muonium calculations we find no level crossings. Since the positronium states show level crossing for states unaffected by the new sector interactions, the origin of this improved behavior may arise from improved computational libraries or the larger N values utilized.

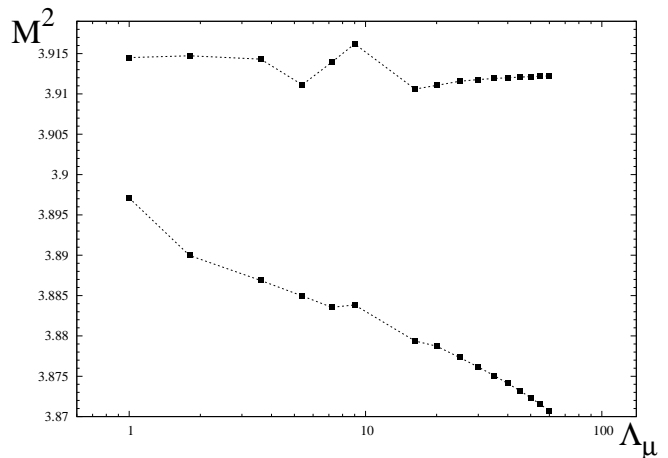


FIG. 1. Mass eigenvalues of $n = 1$ true muonium states with $J_z = 0$ ($1^3S_1^0$ at top, $1^1S_0^0$ at bottom) as a function of cutoff Λ_μ for $\Lambda_e = \frac{m_e}{m_\mu} \Lambda_\mu$, $\alpha = 0.3$, $m_e = \frac{1}{2}m_\mu$, $N = 25$. Both Λ 's are given in units of the muon Bohr momentum $\alpha m_\mu/2$.

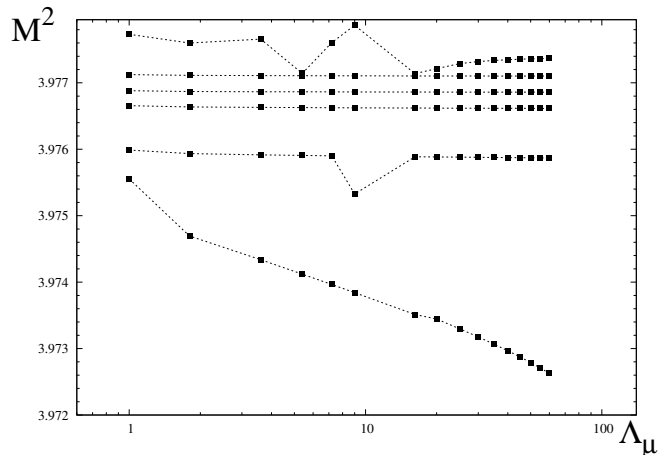


FIG. 2. Mass eigenvalues of $n = 2$ true muonium states with $J_z = 0$ (top to bottom: $2^3S_1^0$, $2^3P_2^0$, $2^1P_1^0$, $2^3P_1^0$, $2^3P_0^0$, $2^1S_0^0$) as a function of cutoff Λ_μ for $\Lambda_e = \frac{m_e}{m_\mu} \Lambda_\mu$, $\alpha = 0.3$, $m_e = \frac{1}{2}m_\mu$, $N = 25$. Both Λ 's are given in units of the muon Bohr momentum $\alpha m_\mu/2$.

On the other hand, new features seen here and not in Ref. [14] include strong fluctuations in the invariant mass in the range $5 \leq \Lambda_\mu \leq 11$ for the given values of N , particularly for triplet states (which couple most strongly to the $|\gamma\rangle$ and $|e\bar{e}\rangle$ states). As mentioned in Sec. III, use of the weighting function $f(\mu)$ defined in Eq. (15) for a fixed Λ means that increasing the value of N samples the regions around $x = 0$, $\frac{1}{2}$, and 1 more heavily, which is particularly significant when the wave functions become small in those neighborhoods. Indeed, the precise nature of the fluctuations changes significantly with N , indicating that the inclusion of the $|e\bar{e}\rangle$ states in some regions is not under perfect numerical control.

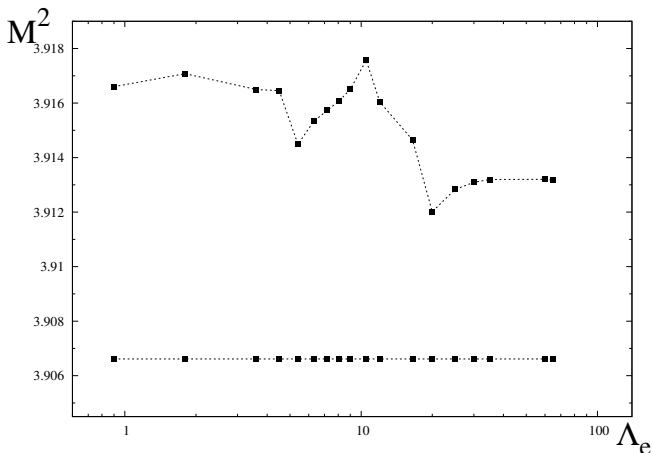


FIG. 3. Mass eigenvalues of $n = 1$ true muonium states with $J_z = 0$ ($1^3S_1^0$ at top, $1^1S_0^0$ at bottom) as a function of cutoff Λ_e for $\Lambda_\mu = m_\mu$, $\alpha = 0.3$, $m_e = \frac{1}{2}m_\mu$, $N = 25$. Both Λ 's are given in units of the muon Bohr momentum $\alpha m_\mu/2$.

As noted above, changing Λ_e in the numerical calculations amounts to changing the Fock states included. If Λ_e and $N_{\mu,\theta}$ are not properly tuned, the continuum $e\bar{e}$ components of the true muonium wave function can be incorrectly suppressed, in that regions of large $e\bar{e}$ amplitude can be numerically undersampled. This suppression of the continuum $e\bar{e}$ components is responsible for the irregular dependence of M^2 upon Λ_e , and hence for this cutoff scheme, upon Λ_μ . Additionally, a comparison of the triplet state masses with those of Ref. [14] shows a weaker dependence in our case for large Λ_μ values.

Since the optimal method of renormalization remains unknown to us, we study its effects by varying Λ_e for a fixed $\Lambda_\mu = \alpha m_\mu/2$. For the range of $0.9 \leq \Lambda_e \leq 65$ in units of the muon Bohr momentum $\alpha m_\mu/2$, we plot this dependence of the $n = 1$ states in Fig. 3. In this regime, we find that Λ_e does not affect singlet M^2 values. On the other hand, we find that the choice of Λ_e can shift the triplet state invariant masses by $\pm 0.002m_\mu^2$. Since corrections to the invariant mass from the $|e\bar{e}\rangle$ sector should be $\approx \alpha^5 m_\mu^2 = 0.003m_\mu^2$, this level of dependence indicates how important establishing a valid prescription for specifying Λ_e will be before the quantitative corrections from the $|e\bar{e}\rangle$ states can be considered reliable at better than an order-of-magnitude level.

VII. RESULTS

Using a version of the code in Ref. [14] modified as discussed above, we compute the entire bound-state spectrum of true muonium and positronium including valence Fock states of both $|\mu\bar{\mu}\rangle$ and $|e\bar{e}\rangle$ for $J_z = -3, -2, \dots, +3$ (e.g., Fig. 4), taking $\alpha = 0.3$ and allowing m_e and the cutoff Λ_e to vary.

From Fig. 4, we see that the true muonium spectrum is

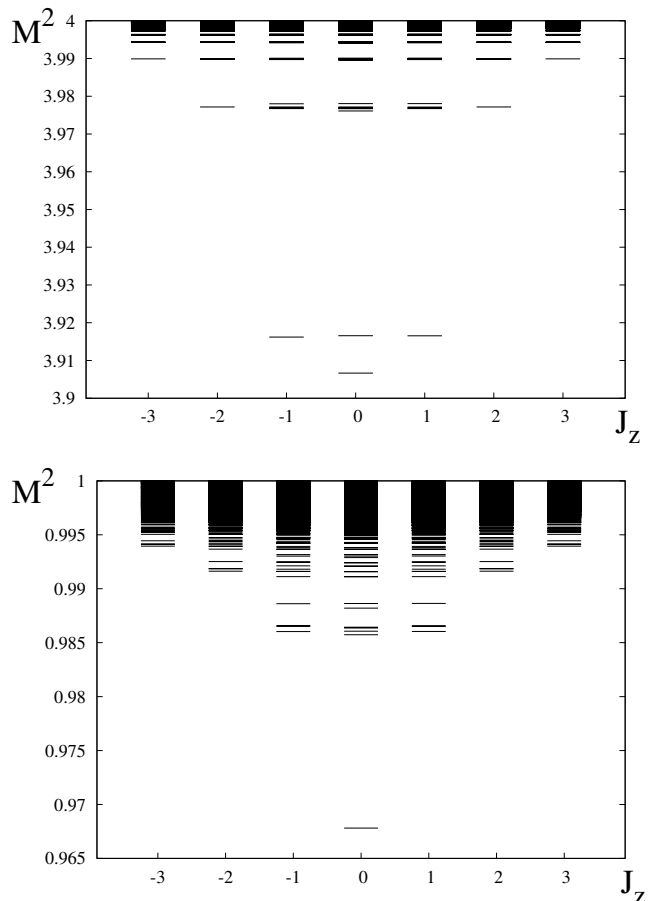


FIG. 4. Spectrum of (top) true muonium and (bottom) positronium with $J_z = -3, -2, \dots, +3$. The spectra are calculated using $\alpha = 0.3$, $m_e = \frac{1}{2}m_\mu$, $\Lambda_\mu = \alpha m_\mu/2$, $\Lambda_e = \alpha m_e/2$, $N = 25$. The mass-squared eigenvalues M_n^2 are expressed in units of m_μ^2 .

nearly identical to that found in [14]. The shifts caused by the inclusion of the $e\bar{e}$ sector are smaller than can be resolved in this plot. In the positronium sector, we notice interesting problems arising from the renormalization procedure. First, the $n = 1$ triplet states have risen in invariant mass to lie nearly degenerate with the $n = 2$ states. States that would be associated with $n = 2$ and $|J_z| = 2$ also have shifted to higher invariant mass, making them difficult to discriminate from the $n = 3$ states. We expect a careful treatment of renormalization to resolve these issues.

Since the two-flavor sectors can only interact through the single-photon annihilation channel, the only true muonium states affected by the inclusion of $|e\bar{e}\rangle$ are those with $|J_z| \leq 1$ [14]. Denoting the bound-state mass-squared eigenvalue before and after including the $e\bar{e}$ states as M_0^2 and $M_{\mu\mu}^2$, respectively, Fig. 5 plots the mass shifts $\Delta M^2 \equiv M_{\mu\mu}^2 - M_0^2$ of $J_z = 0$ true muonium states as a function of m_e in the $n = 1, 2, 3$ energy levels,

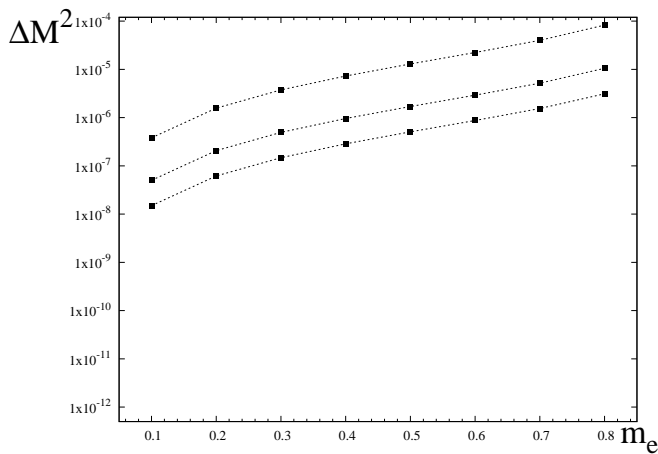


FIG. 5. Eigenvalue shifts $\Delta M^2 \equiv M_{\mu\mu}^2 - M_0^2$ (in units of m_μ^2) for the $n \leq 3$, $J_z = 0$ triplet states of true muonium as functions of m_e , for $\alpha = 0.3$, $\Lambda_\mu = \alpha m_\mu/2$, $\Lambda_e = \alpha m_e/2$, and $N = 23$. From top to bottom, the states are $1^3S_1^0$, $2^3S_1^0$, and $3^3S_1^0$.

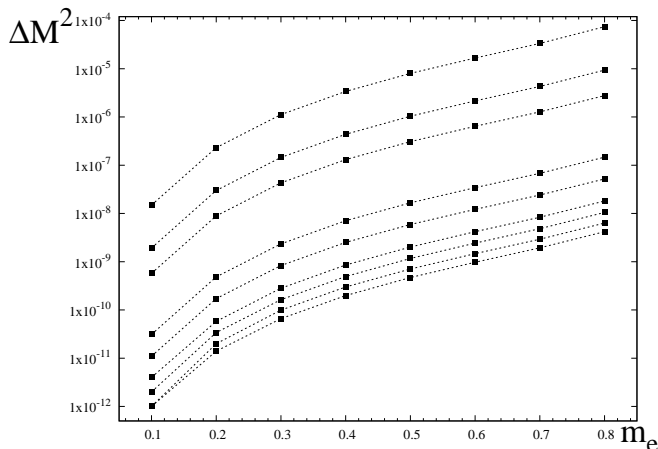


FIG. 6. Eigenvalue shifts $\Delta M^2 \equiv M_{\mu\mu}^2 - M_0^2$ for the $n \leq 3$, $J_z = -1$ states of true muonium as functions of m_e for $\alpha = 0.3$, $\Lambda_\mu = \alpha m_\mu/2$, $\Lambda_e = \alpha m_e/2$, and $N = 23$. From top to bottom, the states are $1^3S_1^{-1}$, $2^3S_1^{-1}$, $3^3S_1^{-1}$, $2^1P_1^{-1}$, $3^1P_1^{-1}$, $2^3P_2^{-1}$, $2^3P_1^{-1}$, $3^3P_2^{-1}$, and $3^3P_1^{-1}$.

while Fig. 6 shows the $J_z = -1$ case.

For the $J_z = 0$ case, $n^3S_1^0$ are the only states affected by the new sector in a numerically significant way, in agreement with front-form predictions [14]. In the $|J_z| = 1$ cases, the P states are also affected, but at a much lower level. By comparing Figs. 5 and 6, we see that the mass shifts for states differing only in J_z are not the same, reflecting that rotational invariance in the light-front calculation at finite numerical accuracy is not entirely restored. The ordering of shifts from largest to smallest reads

$$n^3S_1 > n^1P_1 > n^3P_2 > n^3P_1, \quad (23)$$

for all cutoff prescriptions investigated.

Our calculations indicate that the ΔM^2 of affected states strongly depends on the cutoff prescription. For the $\Lambda_e = (m_e/m_\mu)\Lambda_\mu$ prescription, we find that ΔM^2 as a function of m_e increases rapidly as $m_e \rightarrow m_\mu$ (roughly $\propto m_e^3$). For this particular choice of m_e -dependent cutoff, the physical effects of changing m_e entangle with those from Λ_e dependence, making interpreting the results difficult. Values $\Lambda_e < 2\Lambda_\mu$ independent of m_e give weaker m_e dependence in ΔM^2 (See Fig. 7) but these prescriptions still do not agree qualitatively with each other. We find, however, that the $\Lambda_e = (m_e/m_\mu)\Lambda_\mu$ and m_e -independent $\Lambda_e < 2\Lambda_\mu$ prescriptions agree that the largest shifts occur for the triplet states $n^3S_1^{J_z}$, and are approximately proportional to $1/n^3$.

The addition of the $|e\bar{e}\rangle$ component should lead to a modification of the Lamb shift (by which we mean the sum of all radiative corrections) proportional to a power of the principal quantum number n . While the quantitative values of these shifts depend strongly upon the renormalization scheme, one might expect their ratios for different states in any single scheme to be less sensitive. To study the Lamb shift modifications, we take the ratio of the mass shifts for different n for 3S_1 , 1P_1 , 3P_2 , and 3P_1 , in the scheme where the cutoffs are fixed by $\Lambda_e = (m_e/m_\mu)\Lambda_\mu$. We define the ratio $r_{nn'}$ for $n' > n$ via

$$r_{nn'} \equiv \frac{\Delta M_n^2}{\Delta M_{n'}^2}. \quad (24)$$

Taking the average of $r_{nn'}$ over all m_e values used for the computations, we determine the leading-order dependence $\Delta M_n^2 \propto n^{-\beta}$ from the relation

$$\ln(r_{nn'}) = -\beta \ln\left(\frac{n}{n'}\right). \quad (25)$$

The results are presented in Table II. We find that $\beta \approx 3$ for 3S_1 states, which agrees with instant-form perturbation theory calculations of Lamb shifts [35]. The other states do not show the conventional Lamb-shift scaling, although we have a smaller number of such states available for study.

$2S+1L_J^{J_z}$	β		
n, n'	1, 2	1, 3	2, 3
$^3S_1^0$	2.937 ± 0.008	2.954 ± 0.007	2.982 ± 0.002
$^3S_1^{-1}$	2.957 ± 0.008	2.970 ± 0.006	2.992 ± 0.003
$^1P_1^{-1}$	–	–	2.556 ± 0.003
$^3P_2^{-1}$	–	–	2.713 ± 0.003
$^3P_1^{-1}$	–	–	2.179 ± 0.003

TABLE II. The exponent β defined in Eq. (25) for different states over the range $0.1 \leq m_e/m_\mu \leq 0.8$. Errors are estimated from the variation in m_e alone.

As discussed in Sec. V, one can compare the results of our simulations to the predictions of nonrelativistic

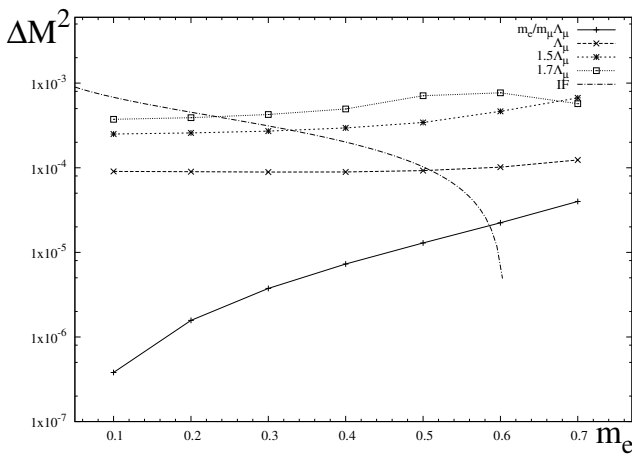


FIG. 7. Eigenvalue shifts $\Delta M^2 \equiv M_{\mu\mu}^2 - M_0^2$ (in units of m_μ^2) for $1^3S_1^0$. The four lines with points correspond to different values of Λ_e . The solid curve is a mass-dependent cutoff, while the other three are fixed ratios of Λ_μ . IF is the instant-form prediction from Eq. (21), using the nonrelativistic wave function. Parameters used are $\alpha = 0.3$, $\Lambda_\mu = \alpha m_\mu/2$, $\Lambda_e = \alpha m_e/2$, and $N = 23$.

instant-form results through Eqs.(17)–(21). Consider, for example, ΔM^2 of $1^3S_1^0$. To account for the strong Λ_e dependence of the shift, we compute ΔM^2 for a few different momentum cutoff prescriptions. These curves are plotted against the instant-form prediction of the VP-e-A diagram in Fig. 7. Clearly, the functional dependence of the instant-form result for VP-e-A is quite different from the results of our simulations, and indeed, using the cutoff prescription $\Lambda_e = (m_e/m_\mu)\Lambda_\mu$ leads to values orders of magnitude smaller than that from the instant form. For the simulations with Λ_e an m_e -independent ratio of Λ_μ , we find a slow increase with m_e . We point out, however, three significant differences between the two calculations. First, the instant-form result here represents only the real part of the energy shift due to vacuum polarization and ignores, for example, vertex corrections. In front form, all of these effects are combined together when one includes explicit $|e\bar{e}\rangle$ and $|e\bar{e}\gamma\rangle$ states. Second, vacuum polarization diagrams in instant form contribute to the renormalization of the coupling constant, an effect not taken into account in this simple model. Finally, a result like Eq. (20) uses only the simplest expression for the nonrelativistic wave function; instant-form calculations that improve upon the nonrelativistic wave function result appear in, *e.g.*, Refs. [36, 37].

Inclusion of the $|e\bar{e}\rangle$ sector also changes the wave functions. One expects that any true muonium bound state contains some component of electron-positron continuum states. The interaction of these states with the true muonium should lead to a modification of the wave functions by means of the $|e\bar{e}\rangle$ component. The $1^3S_1^0$ wave function is expected to be affected the most by the inclusion of the $|e\bar{e}\rangle$. In Fig. 8 we plot the probability density of

the components of the $1^3S_1^0$ state of true muonium using a particular set of parameters. Noting the relative scales, one sees that the antiparallel components dominates the state. As expected for a bound state, the $\mu\bar{\mu}$ pair is localized near $x = \frac{1}{2}$ and $k_\perp \equiv |\mathbf{k}_\perp| = 0$.

The $|e\bar{e}\rangle$ wave function components of this state are expected to appear as continuum states, since the invariant mass $M^2 > 4m_e^2$. From Fig. 8, one sees that the e^+e^- state is sharply peaked along the curve

$$M_S^2 = \frac{m_e^2 + \mathbf{k}_\perp^2}{x(1-x)}, \quad (26)$$

where M_S^2 is the invariant mass of the $1^3S_1^0$ state; the functional sharpness of such components suggests how difficulties in numerical sampling can occur, as discussed in Sec. VI. Additionally, one sees that the fermionic nature of the electrons is manifested most visibly in the parallel spin component, where at $x = \frac{1}{2}$ the probability is heavily suppressed. One also sees that, in agreement with the muonic components, the antiparallel component numerically dominates.

Integrating over the coordinates x, k_\perp , we compile in Table III the integrated probability for each component. From this exercise, we find the surprising result that the antiparallel electronic components contribute more to the wave function than the parallel muonic component. The large uncertainties in the integrated probabilities for the continuum components arise from their sensitive dependence upon Λ_e and N discussed in Sec. VI.

Sector	$\int dx d^2\mathbf{k}_\perp P(x, k_\perp)$
$ \mu\bar{\mu}, \uparrow\uparrow\rangle$	$(2.2 \pm 0.5) \times 10^{-6}$
$ \mu\bar{\mu}, \uparrow\downarrow\rangle$	0.48 ± 0.02
$ e\bar{e}, \uparrow\uparrow\rangle$	$\approx 10^{-6} - 10^{-5}$
$ e\bar{e}, \uparrow\downarrow\rangle$	$\approx 10^{-3} - 10^{-2}$

TABLE III. Integrated probability for each sector in the true muonium $1^3S_1^0$ state. Due to the parity invariance of QED, sectors with both spins flipped have identical probability [*e.g.*, $P(|\mu\bar{\mu}, \uparrow\uparrow\rangle) = P(|\mu\bar{\mu}, \downarrow\downarrow\rangle)$]. The parameters used are $\alpha = 0.3$, $m_e = \frac{1}{2}m_\mu$, $\Lambda_\mu = \alpha m_\mu/2$, $\Lambda_e = 8.0 \cdot \alpha m_e/2$, $N = 27$. Uncertainties are estimated by varying N .

VIII. DISCUSSION AND CONCLUSIONS

In this paper, we have computed the light-front wave functions of true muonium, using a simple model of two-flavor QED that includes a limited number (5) of explicit Fock states. Using this model, we have seen that corrections from $|e\bar{e}\rangle$ have a noticeable effect on true muonium states. The probability density for the first excited state of true muonium, the triplet 1^3S_1 with $J_z = 0$, was determined and the integrated probability for each valence Fock-space component was computed. If m_e is taken to be a substantial fraction of m_μ and the fine structure

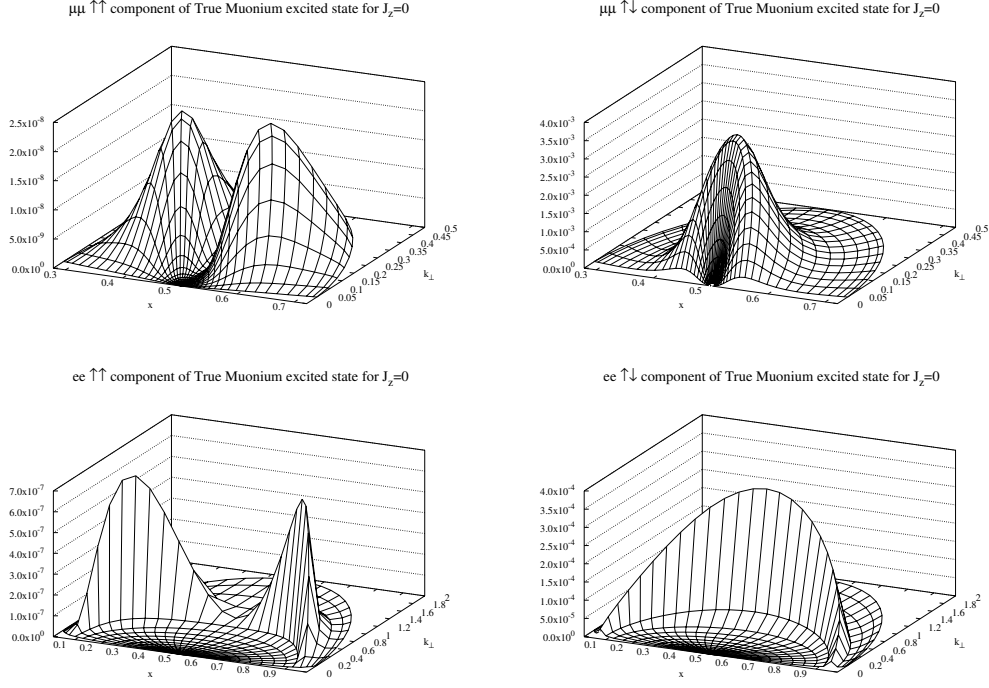


FIG. 8. The first triplet state ($1^3S_1^0$) probability density of the (top left) parallel-helicity muonic, (top right) antiparallel-helicity muonic, (bottom left) parallel-helicity electronic, and (bottom right) antiparallel-helicity electronic components of true muonium with $J_z = 0$, as functions of x and k_\perp , for $\alpha = 0.3$, $m_e = \frac{1}{2}m_\mu$, $\Lambda_\mu = \alpha m_\mu/2$, $\Lambda_e = 8.0 \cdot \alpha m_e/2$, and $N = 27$.

constant is taken large ($\alpha = 0.3$), then the $|e\bar{e}\rangle$ states constitute as much as $O(10^{-2})$ of the true muonium eigenstates.

For a more accurate model, three critical Fock states must also be included: $|\gamma\gamma\rangle$, which dominates the decay of singlet states of true muonium (and in particular should have a pronounced effect on 1S_0 wave functions), and the pair of states $|\mu\bar{\mu}e\bar{e}\rangle$ and $|\mu\bar{\mu}\mu\bar{\mu}\rangle$, which provide crucial contributions to the vacuum polarization corrections. To integrate these states into a model, a proper renormalization of the Hamiltonian is necessary. Methods of interest that have been developed to carry out the renormalization include using Pauli-Villars regulators [29, 30], the Hamiltonian-flow approach [31, 32], and methods with sector-dependent counterterms [33, 34].

In addition to the analytical work required, including these additional Fock states will mandate a much larger numerical effort. While the new states could in principle just be added to the list of valence states included (just as $|e\bar{e}\rangle$ and $|e\bar{e}\gamma\rangle$ are this work), the numerical effort required to accommodate them is likely too great. For example, the sector $|\mu\bar{\mu}e\bar{e}\rangle$ has 6 independent coordinates and 16 spin states. This sector alone would naively require $16 \times N^6$ elements in each eigenvector, a number that is greater than the dimension of the entire Fock space considered in our toy model. Instead, the implementation of these Fock states will likely require developing an appropriate effective interaction for their

successful incorporation into the calculation.

Once the component wave functions are computed by any suitable means, they are ready to incorporate directly into the calculation of any physical process. For example, the dissociative diffraction of pions in the presence of nuclear matter [38] (used to explore QCD color transparency [39]) employs distribution functions that, in the light-front form, are none other than the pion component wave functions [40]. Essentially the same physics, but applied to the much simpler QED case, appears in experiments discussed above [4] that probe the dissociation of true muonium on high- Z targets.

Appendix: Matrix Elements between Flavor Sectors

The relevant matrix elements for the calculation can be obtained through a straightforward generalization of the results in Ref. [14], particularly Appendix F. Those involving a single flavor (μ or e) are exactly the same as in Appendices F.1–F.3, once the appropriate fermion mass is used. Only the single-photon annihilation graphs (App. F.4) that mix the flavors differ. Denoting the initial and final fermion masses as m' , m , respectively (and similarly for x and k_\perp), the key kinematic quantity ap-

pearing in the propagators is the effective kinetic energy

$$\omega^* \equiv \frac{1}{2} \left[\frac{m^2 + k_\perp^2}{x(1-x)} + \frac{m'^2 + k'_\perp^2}{x'(1-x')} \right], \quad (\text{A.1})$$

which is a slightly different ω^* than is used for the standard annihilation graphs in the absence of $e\bar{e}$. This definition in either case has the special significance in the method of iterated resolvents, that it allows the truncation of neglected Fock states in a controlled manner. The amplitudes for the process then read:

$$I_1(x, k_\perp; x', k'_\perp) = \frac{\alpha}{\pi} \frac{2m'm}{\omega^*} \frac{1}{x(1-x)} \frac{1}{x'(1-x')} \delta_{|J_z|,1}, \quad (\text{A.2})$$

$$I_2(x, k_\perp; x', k'_\perp) = \frac{\alpha}{\pi} \left[\frac{2}{\omega^*} \frac{k_\perp k'_\perp}{xx'} \delta_{|J_z|,1} + 4\delta_{J_z,0} \right], \quad (\text{A.3})$$

$$I_3(x, k_\perp; x', k'_\perp) = \frac{\alpha}{\pi} \frac{2m\lambda_1}{\omega^*} \frac{1}{x(1-x)} \frac{k'_\perp}{1-x'} \delta_{|J_z|,1}, \quad (\text{A.4})$$

$$I_4(x, k_\perp; x', k'_\perp) = -\frac{\alpha}{\pi} \left[\frac{2}{\omega^*} \frac{k_\perp k'_\perp}{x'(1-x)} \delta_{|J_z|,1} - 4\delta_{J_z,0} \right]. \quad (\text{A.5})$$

Note that the only nonvanishing matrix elements have $|J_z| \leq 1$, a restriction due to the angular momentum of the photon. Abbreviating $I_i(1, 2) \equiv I_i(x, k_\perp; x', k'_\perp)$, the amplitudes for all allowed combinations of helicity states are given in Table IV.

$m : m'$	$\uparrow\uparrow$	$\uparrow\downarrow$	$\downarrow\uparrow$	$\downarrow\downarrow$
$\uparrow\uparrow$	$I_1(1, 2)$	$I_3(2, 1)$	$I_3^*(2, 1)$	0
$\uparrow\downarrow$	$I_3(1, 2)$	$I_2^*(1, 2)$	$I_4(2, 1)$	0
$\downarrow\uparrow$	$I_3^*(1, 2)$	$I_4(1, 2)$	$I_2(1, 2)$	0
$\downarrow\downarrow$	0	0	0	0

TABLE IV. Helicity table of the annihilation graph, where m and m' indicate the final-state and initial-state fermions, respectively.

ACKNOWLEDGMENTS

We thank S. Brodsky for very useful conversations, and H.L. thanks U. Trittman for valuable insight into understanding his code. This work was supported by the National Science Foundation under Grant No. PHY-1068286.

-
- [1] R. Coombes, R. Flexer, A. Hall, R. Kennelly, J. Kirkby, R. Piccioni, D. Porat and M. Schwartz *et al.*, Phys. Rev. Lett. **37**, 249 (1976).
- [2] D.B. Cassidy and A.P. Mills, Nature (London) **449**, 195 (2007).
- [3] S.J. Brodsky and R.F. Lebed, Phys. Rev. Lett. **102**, 213401 (2009) [arXiv:0904.2225 [hep-ph]].
- [4] A. Banburski and P. Schuster, Phys. Rev. D **86**, 093007 (2012) [arXiv:1206.3961 [hep-ph]].
- [5] A. Antognini, F. Nez, K. Schuhmann, F.D. Amaro, F. Biraben, J.M.R. Cardoso, D.S. Covita and A. Dax *et al.*, Science **339**, 417 (2013).
- [6] D. Tucker-Smith and I. Yavin, Phys. Rev. D **83**, 101702 (2011) [arXiv:1011.4922 [hep-ph]].
- [7] R.T. Robiscoe, Phys. Rev. **138**, A22 (1965).
- [8] P.A.M. Dirac, Rev. Mod. Phys. **21**, 392 (1949).
- [9] S.J. Brodsky, H.-C. Pauli and S.S. Pinsky, Phys. Rept. **301**, 299 (1998) [hep-ph/9705477].
- [10] H.C. Pauli and S.J. Brodsky, Phys. Rev. D **32**, 2001 (1985).
- [11] A.C. Tang, S.J. Brodsky and H.C. Pauli, "electrodynamics," Phys. Rev. D **44**, 1842 (1991).
- [12] M. Krautgartner, H.C. Pauli and F. Wolz, Phys. Rev. D **45**, 3755 (1992).
- [13] M. Kaluža and H.C. Pauli, Phys. Rev. D **45**, 2968 (1992).
- [14] U. Trittman and H.-C. Pauli, hep-th/9704215.
- [15] S.J. Brodsky, R. Roskies and R. Suaya, Phys. Rev. D **8**, 4574 (1973).
- [16] H. Lamm and R.F. Lebed, in preparation.
- [17] G.P. Lepage and S.J. Brodsky, Phys. Rev. D **22**, 2157 (1980).
- [18] I. Tamm, J. Phys. (USSR) **9**, 449 (1945).
- [19] S.M. Dancoff, Phys. Rev. **78**, 382 (1950).
- [20] H.-C. Pauli, hep-th/9608035.
- [21] U. Trittman, in *Les Houches 1997, New non-perturbative methods and quantization on the light cone*, pp. 89-96 [hep-th/9706055].
- [22] U. Trittman, hep-th/9705072.
- [23] U. Trittman and H.-C. Pauli, Nucl. Phys. Proc. Suppl. **90**, 161 (2000).
- [24] H.-C. Pauli, in *Nagoya 1996, Perspectives of strong coupling gauge theories*, pp. 342-352 [hep-th/9706036].
- [25] U.D. Jentschura, G. Soff, V.G. Ivanov and S.G. Karshenboim, Phys. Rev. A **56**, 4483 (1997) [physics/9706026].
- [26] B.D. Jones, R.J. Perry and S.D. Glazek, Phys. Rev. D **55**, 6561 (1997) [hep-th/9605231].
- [27] B.D. Jones, hep-th/9703106.
- [28] R. Karplus and A. Klein, Phys. Rev. **87**, 848 (1952).
- [29] S.S. Chabysheva and J.R. Hiller, Phys. Rev. D **81**, 074030 (2010) [arXiv:0911.4455 [hep-ph]].
- [30] S.S. Chabysheva and J.R. Hiller, Phys. Rev. D **82**, 034004 (2010) [arXiv:1006.1077 [hep-ph]].

- [31] E.L. Gubankova, H.-C. Pauli and F.J. Wegner, hep-th/9809143.
- [32] E.L. Gubankova and G. Papp, hep-th/9904081.
- [33] V.A. Karmanov, J.-F. Mathiot and A.V. Smirnov, Phys. Rev. D **77**, 085028 (2008) [arXiv:0801.4507 [hep-th]].
- [34] V.A. Karmanov, J.F. Mathiot and A.V. Smirnov, Phys. Rev. D **86**, 085006 (2012) [arXiv:1204.3257 [hep-th]].
- [35] C. Itzykson and J.-B. Zuber, *Quantum Field Theory*, McGraw-Hill, New York (1980).
- [36] D. Eiras and J. Soto, Phys. Lett. B **491**, 101 (2000) [hep-ph/0005066].
- [37] V.G. Ivanov, E.Y. Korzinin and S.G. Karshenboim, Phys. Rev. D **80**, 027702 (2009).
- [38] L. Frankfurt, G.A. Miller and M. Strikman, Phys. Lett. B **304**, 1 (1993) [hep-ph/9305228].
- [39] E.M. Aitala *et al.* [E791 Collaboration], Phys. Rev. Lett. **86**, 4773 (2001) [hep-ex/0010044].
- [40] D. Ashery, Prog. Part. Nucl. Phys. **56**, 279 (2006).